Hindawi
Advances in High Energy Physics
Volume 2018, Article ID 6031362, 17 pages
https://doi.org/10.1155/2018/6031362

Research Article

Novel Neutrino-Floor and Dark Matter Searches with Deformed Shell Model Calculations

D. K. Papoulias,[1] **R. Sahu**,[2] **T. S. Kosmas**,[3] **V. K. B. Kota**,[4] **and B. Nayak**[2]

[1] *Institute of Nuclear and Particle Physics, NCSR 'Demokritos', 15310 Agia Paraskevi, Greece*
[2] *National Institute of Science and Technology, Palur Hills, Berhampur, Odisha 761008, India*
[3] *Theoretical Physics Section, University of Ioannina, 45110 Ioannina, Greece*
[4] *Physical Research Laboratory, Ahmedabad 380 009, India*

Correspondence should be addressed to D. K. Papoulias; dimpap@cc.uoi.gr

Received 15 May 2018; Revised 16 July 2018; Accepted 9 August 2018; Published 26 August 2018

Academic Editor: Enrico Lunghi

 The publication of this article was funded by SCOAP[3].

Event detection rates for WIMP-nucleus interactions are calculated for ^{71}Ga, ^{73}Ge, ^{75}As, and ^{127}I (direct dark matter detectors). The nuclear structure form factors, which are rather independent of the underlying beyond the Standard Model particle physics scenario assumed, are evaluated within the context of the deformed nuclear shell model (DSM) based on Hartree-Fock nuclear states. Along with the previously published DSM results for ^{73}Ge, the neutrino-floor due to coherent elastic neutrino-nucleus scattering (CEνNS), an important source of background to dark matter searches, is extensively calculated. The impact of new contributions to CEνNS due to neutrino magnetic moments and Z' mediators at direct dark matter detection experiments is also examined and discussed. The results show that the neutrino-floor constitutes a crucial source of background events for multi-ton scale detectors with sub-keV capabilities.

1. Introduction

In the last few decades, the measurements of the cosmic microwave background (CMB) radiation offered a remarkably powerful way of modelling the origin of cosmic-ray anisotropies and constraining the geometry, the evolution, and the matter content of our universe. Such observations have in general indicated the consistency of the standard cosmological model [1] and the fact that our universe hardly contains ~ 5% luminous matter, whereas the remainder consists of nonluminous dark matter (~ 23%) and dark energy (~ 72%) [2]. After the discovery of the CMB fluctuations by the Cosmic Background Explorer (COBE) satellite [3], the extremely high precision of the WMAP satellite and especially of the Planck third-generation space mission has helped us to produce maps for the CMB anisotropies and other cosmological parameters (see [4] for details). We also mention that high-resolution ground-based CMB data, like those of the Atacama Cosmology Telescope (ACT) [5] and the South Pole Telescope (SPT) [6] have recovered the underlying CMB spectra observed by the space missions.

Focusing on the topic we address in this work, it is worth noting that the CMB data, the Supernova Cosmology project [7], and so on suggest that most of the dark matter of the universe is cold. Furthermore, the baryonic cold dark matter (CDM) component can be considered to consist of either massive compact halo objects (MACHOs) like neutron stars, white dwarfs, Jupiters, etc. or Weakly Interacting Massive Particles (WIMPs) that constantly bombard Earth's atmosphere. Several results of experimental searches suggest that the MACHO fraction should not exceed a portion of about 20% [1]. On the theoretical side, within the framework of new physics beyond the Standard Model (SM), supersymmetric (SUSY) theories provide promising nonbaryonic candidates for dark matter [8] (for a review see [9]). In the simple picture, the dark matter in the galactic halo is assumed to be Weakly Interacting Massive Particles (WIMPs). The most appealing WIMP candidate for nonbaryonic CDM is the

lightest supersymmetric particle (LSP) which is expected to be a neutral Majorana fermion traveling with nonrelativistic velocities [10].

In recent years, there have been considerable theoretical and experimental efforts towards WIMP detection through several nuclear probes [11–13]. Popular target nuclei include among others the ^{71}Ga, ^{73}Ge, ^{75}As, ^{127}I, ^{134}Xe, and ^{208}Pb isotopes [14, 15]. Towards the first ever dark matter detection, a great number of experimental efforts take place aiming at measuring the energy deposited after the galactic halo WIMPs scatter off the nuclear isotopes of the detection material. Because of the low count rates, due to the fact that the WIMP-nucleus interaction is remarkably weak, the choice of the detector plays very important role and for this reason spin-dependent interactions require the use of targets with nonzero spin. The Cryogenic Dark Matter Search (CDMS) experimental facility [16] has been designed to directly detect the dark matter by employing a ^{73}Ge as the target nucleus, setting the most sensitive limits on the interaction of WIMP with terrestrial materials to date. The development of upgrades is under way and will be located at SNOLAB. Another prominent dark matter experiment is the EDELWEISS facility in France [17] which uses high purity germanium cryogenic bolometers at milli-Kelvin temperatures. There are also other experimental attempts using detectors like ^{127}I, ^{129,131}Xe, ^{133}Cs, etc. (see [18–20]).

Inevitably, direct detection experiments are exposed to various neutrino emissions, such as those originating from astrophysical sources (e.g., Solar [21], Atmospheric [22, 23], and diffuse Supernova [24] neutrinos), Earth neutrinos (Geoneutrinos [25]), and in other cases even artificial terrestrial neutrinos (e.g., neutrinos from nearby reactors [26]). The subsequent neutrino interactions with the material of dark matter detectors, namely, the neutrino-floor, may perfectly mimic possible WIMP signals [27]. Thus, the impacts of the neutrino-floor on the relevant experiments looking for CDM as well as on the detector responses to neutrino interactions need be comprehensively investigated. Since Geoneutrino fluxes are relatively low, astrophysical neutrinos are recognised as the most significant background source that remains practically irreducible [28]. The recent advances of direct detection dark matter experiments, mainly due to the development of low threshold technology and high detection efficiency, are expected to reach the sensitivity frontiers in which astrophysical neutrino-induced backgrounds are expected to limit the observation potential of the WIMP signal [29].

In this work, we explore the impact of the most important neutrino background source on the relevant direct dark matter detection experiments by concentrating on the dominant neutrino-matter interaction channel, e.g., the coherent elastic neutrino-nucleus scattering (CEνNS) [30, 31]. It is worthwhile to mention that events of this process were recently measured for the first time by the COHERENT experiment at the Spallation Neutrino Source [32], completing the SM picture of electroweak interactions at low energies. Such a profound discovery motivated our present work and we will make an effort to shed light on the nuclear physics aspects. Neutrino nonstandard interactions (NSIs) [33] may constitute an important source of neutrino background and have been investigated recently in [34, 35]. Thus, apart from addressing the SM contributions to CEνNS [36], we also explore the impact of new physics contributions that arise in the context of electromagnetic (EM) neutrino properties [37, 38] as well as of those emerging in the framework of $U(1)'$ gauge interactions [39] due to the presence of new light Z' mediators [40, 41]. The aforementioned interaction channels may lead to a novel neutrino-floor as demonstrated by [42]. The latter could be detectable in view of the constantly increasing sensitivity of the upcoming direct detection experiments with multi-ton mass scale and sub-keV capabilities [43].

Direct detection dark matter experiments are currently entering a precision era, and nuclear structure effects are expected to become rather important and should be incorporated in astroparticle physics applications [45]. For this reason, our nuclear model is at first tested in its capabilities to adequately describe the nuclear properties before being applied to problems like dark matter detection. This work considers the deformed shell model (DSM), on the basis of Hartree-Fock (HF) deformed intrinsic states with angular momentum projection and band mixing [46], all with a realistic effective interaction and a set of single-particle states and single-particle energies, which is established to be rather successful in describing the properties of nuclei in the mass range $A = 60$–90 (see [47] for details regarding DSM and its applications). In particular, the DSM is employed for calculating the required nuclear structure factors entering the dark matter and neutrino-floor expected event rates by focusing on four interesting nuclei regarding dark matter investigations such as ^{71}Ga, ^{73}Ge, ^{75}As, and ^{127}I. Let us add that details of nuclear structure and dark matter event rates for ^{73}Ge obtained using DSM have been reported recently [48].

The paper has been organised as follows. Section 2 gives the main ingredients of WIMP-nucleus scattering, while Section 3 provides the formulation for neutrino-nucleus scattering (neutrino-floor) within and beyond the SM. Then in Section 4 we describe briefly the methodology of the DSM, and the main results of the present work are presented and discussed in Section 5. Finally, the concluding remarks are drawn in Section 6.

2. Searching WIMP Dark Matter

The Earth is exposed to a huge number of WIMPs originating from the galactic halo. Their direct detection through nuclear recoil measurements after scattering off the target nuclei at the relevant dark matter experiments is of fundamental interest in modern physics and is expected to have a direct impact on astroparticle physics and cosmology. In this section we discuss the mathematical formulation of WIMP-nucleus scattering. The formalism introduces an appropriate separation of the SUSY and nuclear parts entering the event rates of WIMP-nucleus interactions in our effort to emphasise the important role played by the nuclear physics aspects. In particular we perform reliable nuclear structure calculations within the context of DSM based on Hartree-Fock states.

2.1. WIMP-Nucleus Scattering. For direct detection dark matter experiments, the differential event rate of a WIMP with mass m_χ scattering off a nucleus (A, Z) with respect to the momentum transfer q can be cast in the form [1]

$$\frac{dR(u,v)}{dq^2} = N_t \phi \frac{d\sigma}{dq^2} f(v)\, d^3v, \tag{1}$$

where $N_t = 1/(Am_p)$ denotes the number of target nuclei per unit mass, A stands for the mass number of the target nucleus, and m_p is the proton mass. In the above expression the WIMP flux is $\phi = \rho_0 v/m_\chi$, with ρ_0 being the local WIMP density. The distribution of WIMP velocity relative to the detector (or Earth) and also the motion of the Sun and Earth, $f(v)$, is taken into account and assumed to resemble a Maxwell-Boltzmann distribution to ensure consistency with the LSP velocity distribution. Note that, by neglecting the rotation of Earth in its own axis, $v = |\mathbf{v}|$ accounts for the relative velocity of WIMP with respect to the detector. For later convenience a dimensionless variable $u = q^2b^2/2$ is introduced with b denoting the oscillator length parameter, and the corresponding WIMP-nucleus differential cross section in the laboratory frame reads [10, 15, 48–50]

$$\frac{d\sigma(u,v)}{du} = \frac{1}{2}\sigma_0 \left(\frac{1}{m_p b}\right)^2 \frac{c^2}{v^2} \frac{d\sigma_A(u)}{du}, \tag{2}$$

with

$$\begin{aligned}\frac{d\sigma_A}{du} = {} & \left[f_A^0 \Omega_0(0)\right]^2 F_{00}(u) \\ & + 2 f_A^0 f_A^1 \Omega_0(0)\, \Omega_1(0)\, F_{01}(u) \\ & + \left[f_A^1 \Omega_1(0)\right]^2 F_{11}(u) + \mathscr{M}^2(u).\end{aligned} \tag{3}$$

The first three terms account for the spin contribution due to the axial current, while the fourth term accounts for the coherent contribution arising from the scalar interaction. The coherent contribution is expressed in terms of the nuclear form factors given as

$$\begin{aligned}\mathscr{M}^2(u) = {} & \left(f_S^0 \left[Z F_Z(u) + N F_N(u)\right]\right. \\ & \left. + f_S^1 \left[Z F_Z(u) - N F_N(u)\right]\right)^2.\end{aligned} \tag{4}$$

The coherent part in the approximation of nearly equal proton and neutron nuclear form factors $F_Z(u) \approx F_N(u)$ is given as

$$\mathscr{M}^2(u) = A^2 \left(f_S^0 - f_S^1 \frac{A-2Z}{A}\right)^2 |F(u)|^2. \tag{5}$$

The respective values of the nucleonic-current parameters f_V^0, f_V^1 for the isoscalar and isovector parts of the vector current (not shown here), f_A^0, f_A^1 for the isoscalar and isovector parts of the axial-vector current, and f_S^0, f_S^1 for the isoscalar and isovector parts of the scalar current depend on the specific SUSY model employed [51]. The spin structure functions $F_{\rho\rho'}(u)$ with $\rho, \rho' = 0, 1$ for the isoscalar and isovector contributions, respectively, take the form

$$F_{\rho\rho'}(u) = \sum_{\lambda,\kappa} \frac{\Omega_\rho^{(\lambda,\kappa)}(u)\, \Omega_{\rho'}^{(\lambda,\kappa)}(u)}{\Omega_\rho(0)\, \Omega_{\rho'}(0)}, \tag{6}$$

with

$$\begin{aligned}\Omega_\rho^{(\lambda,\kappa)}(u) = {} & \sqrt{\frac{4\pi}{2J_i+1}} \times \left\langle J_f \right| | \\ & \sum_{j=1}^{A} \left[Y_\lambda(\Omega_j) \otimes \sigma(j)\right]_\kappa j_\lambda\left(\sqrt{u} r_j\right) \omega_\rho(j) \, | \, |J_i\rangle.\end{aligned} \tag{7}$$

Here, $\omega_0(j) = 1$ and $\omega_1(j) = \tau(j)$ with $\tau = +1$ for protons and $\tau = -1$ for neutrons, while Ω_j represents the solid angle for the position vector of the j-th nucleon and j_λ stands for the well-known spherical Bessel function. The quantities $\Omega_\rho(0) = \Omega_\rho^{(0,1)}(0)$ are the static spin matrix elements (see, e.g., [8]). In this context, the WIMP-nucleus event rate per unit mass of the detector is conveniently written as

$$\begin{aligned}\langle R \rangle = {} & \left(f_A^0\right)^2 D_1 + 2 f_A^0 f_A^1 D_2 + \left(f_A^1\right)^2 D_3 \\ & + A^2 \left(f_S^0 - f_S^1 \frac{A-2Z}{A}\right)^2 |F(u)|^2 D_4.\end{aligned} \tag{8}$$

The functions D_i enter the definition of the WIMP-nucleus event rate through the three-dimensional integrals, given by

$$D_i = \int_{-1}^{1} d\xi \int_{\psi_{\min}}^{\psi_{\max}} d\psi \int_{u_{\min}}^{u_{\max}} G(\psi, \xi)\, X_i\, du, \tag{9}$$

with

$$\begin{aligned}X_1 &= \left[\Omega_0(0)\right]^2 F_{00}(u), \\ X_2 &= \Omega_0(0)\, \Omega_1(0)\, F_{01}(u), \\ X_3 &= \left[\Omega_1(0)\right]^2 F_{11}(u), \\ X_4 &= |F(u)|^2.\end{aligned} \tag{10}$$

In the latter expression, D_1, D_2, and D_3 account for the spin-dependent parts of (3), while D_4 is associated with the coherent contribution.

In this work, the nuclear wave functions $\langle J_f|$ and $|J_i\rangle$ entering (7) are calculated within the nuclear DSM of [46, 47]. For a comprehensive discussion on the explicit form of the function $G(\psi)$, the integration limits of (9) and the various parameters entering into these, the reader is referred to [48].

3. Neutrino-Nucleus Scattering

The neutrino-floor stands out as an important source of irreducible background to WIMP searches at a direct detection experiment. In this work we explore the neutrino-floor due to neutrino-nucleus scattering since the corresponding floor

Table 1: Solar neutrino fluxes and uncertainties in the framework of the employed high metallicity SSM (for details, see the text).

type	$E_{\nu_{\max}}$ [MeV]	flux [$\mathrm{cm}^{-2}\mathrm{s}^{-1}$]
pp	0.423	$(5.98 \pm 0.006) \times 10^{10}$
pep	1.440	$(1.44 \pm 0.012) \times 10^{8}$
hep	18.784	$(8.04 \pm 1.30) \times 10^{3}$
$^{7}\mathrm{Be}_{\mathrm{low}}$	0.3843	$(4.84 \pm 0.48) \times 10^{8}$
$^{7}\mathrm{Be}_{\mathrm{high}}$	0.8613	$(4.35 \pm 0.35) \times 10^{9}$
$^{8}\mathrm{B}$	16.360	$(5.58 \pm 0.14) \times 10^{6}$
$^{13}\mathrm{N}$	1.199	$(2.97 \pm 0.14) \times 10^{8}$
$^{15}\mathrm{O}$	1.732	$(2.23 \pm 0.15) \times 10^{8}$
$^{17}\mathrm{F}$	1.740	$(5.52 \pm 0.17) \times 10^{6}$

coming from neutrino-electron scattering is relatively low [52]. Motivated by the novel neutrino interaction searches using reactor neutrinos of [42], here we consider various astrophysical neutrino sources in our calculations that involve the conventional and beyond the SM interactions channels (see below).

3.1. Differential Event Rate at Dark Matter Detectors. For a given interaction channel $x = \mathrm{SM}, \mathrm{EM}, Z'$, the differential event rate dR_ν/dT_N of CEνNS processes at a dark matter detector is obtained through the convolution of the normalised neutrino energy distribution $\lambda_\nu(E_\nu)$ of the background neutrino source in question (i.e., Solar, Atmospheric and Diffuse Supernova Neutrinos, as seen below) with the CEνNS cross section, as follows [53]:

$$\left(\frac{dR_\nu}{dT_N}\right)_{\mathrm{x}} = \mathscr{K} \int_{E_\nu^{\min}}^{E_\nu^{\max}} \lambda_\nu(E_\nu) \frac{d\sigma_{\mathrm{x}}}{dT_N}(E_\nu, T_N)\, dE_\nu, \tag{11}$$

where $E_\nu^{\max}$ is the maximum neutrino energy of the source in question (for the case of Solar neutrinos see, e.g., Table 1) and $E_\nu^{\min} = \sqrt{MT_N/2}$ is the minimum neutrino energy that is required to yield a nuclear recoil with energy T_N. In the latter expression $\mathscr{K} = t_{\mathrm{run}} N_{\mathrm{targ}} \Phi_\nu$ with t_{run} being the exposure time, N_{targ} is the number of target nuclei and Φ_ν is the assumed neutrino flux.

3.1.1. Standard Model Interactions. Assuming SM interactions only, at low and intermediate neutrino energies $E_\nu \ll M_W$, the weak neutral-current CEνNS process is adequately described by the four-fermion effective interaction Lagrangian [33, 36]

$$\mathscr{L}_{\mathrm{SM}} = -2\sqrt{2} G_F \sum_{\substack{f=u,d \\ \alpha=e,\mu,\tau}} g_{\alpha\alpha}^{f,P} \left[\overline{\nu}_\alpha \gamma_\rho L \nu_\alpha\right] \left[\overline{f} \gamma^\rho P f\right], \tag{12}$$

where $P = \{L, R\}$ denote the chiral projectors, $\alpha = \{e, \mu, \tau\}$ represents the neutrino flavour, and $f = \{u, d\}$ is a first generation quark. By including the radiative corrections of [54], the P-handed couplings of the f quarks to the Z-boson are expressed as

$$\begin{aligned}
g_{\alpha\alpha}^{u,L} &= \rho_{\nu N}^{NC}\left(\frac{1}{2} - \frac{2}{3}\widehat{\kappa}_{\nu N}\widehat{s}_Z^2\right) + \lambda^{u,L}, \\
g_{\alpha\alpha}^{d,L} &= \rho_{\nu N}^{NC}\left(-\frac{1}{2} + \frac{1}{3}\widehat{\kappa}_{\nu N}\widehat{s}_Z^2\right) + \lambda^{d,L}, \\
g_{\alpha\alpha}^{u,R} &= \rho_{\nu N}^{NC}\left(-\frac{2}{3}\widehat{\kappa}_{\nu N}\widehat{s}_Z^2\right) + \lambda^{u,R}, \\
g_{\alpha\alpha}^{d,R} &= \rho_{\nu N}^{NC}\left(\frac{1}{3}\widehat{\kappa}_{\nu N}\widehat{s}_Z^2\right) + \lambda^{d,R},
\end{aligned} \tag{13}$$

with $\widehat{s}_Z^2 = \sin^2\theta_W = 0.2312$, $\rho_{\nu N}^{NC} = 1.0086$, $\widehat{\kappa}_{\nu N} = 0.9978$, $\lambda^{u,L} = -0.0031$, $\lambda^{d,L} = -0.0025$, and $\lambda^{d,R} = 2\lambda^{u,R} = 7.5\times10^{-5}$.

In this work we restrict our study only to low momentum transfer in order to satisfy the coherent condition $|\mathbf{q}| \leq 1/R_A$, where R_A is the nuclear size and $|\mathbf{q}|$ is the magnitude of the three-momentum transfer [31]. Focusing on the dominant CEνNS channel, the relevant SM differential cross section with respect to the nuclear recoil energy T_N takes the form [41]

$$\begin{aligned}
\frac{d\sigma_{\mathrm{SM}}}{(dT_N)}(E_\nu, T_N) = \frac{G_F^2 M}{\pi}\Bigg[&\left(\mathcal{Q}_W^V\right)^2\left(1 - \frac{MT_N}{2E_\nu^2}\right) \\
&+ \left(\mathcal{Q}_W^A\right)^2\left(1 + \frac{MT_N}{2E_\nu^2}\right)\Bigg],
\end{aligned} \tag{14}$$

with E_ν denoting the neutrino energy and M the mass of the target nucleus. The relevant vector ($\mathcal{Q}_W^V$) and axial-vector ($\mathcal{Q}_W^A$) weak charges entering the CEνNS cross section are given by the relations [55]

$$\begin{aligned}
\mathcal{Q}_W^V\left(Q^2\right) &= \left[g_p^V Z F_Z^V\left(Q^2\right) + g_n^V N F_N^V\left(Q^2\right)\right], \\
\mathcal{Q}_W^A\left(Q^2\right) &= \left[g_p^A\left(Z_+ - Z_-\right) + g_n^A\left(N_+ - N_-\right)\right] F_A\left(Q^2\right).
\end{aligned} \tag{15}$$

Here, $Z_\pm$ ($N_\pm$) stands for the number of protons (neutrons) with spin up (+) and spin down (−), respectively, while g_p^A

(g_n^A) represent the axial-vector couplings of protons (neutrons) to the Z^0 boson. At the nuclear level, the relevant vector (axial-vector) couplings of protons g_p^V (g_p^A) and neutrons g_n^V (g_n^A) take the form

$$\begin{aligned} g_p^V &= 2\left(g_{\alpha\alpha}^{u,L} + g_{\alpha\alpha}^{u,R}\right) + \left(g_{\alpha\alpha}^{d,L} + g_{\alpha\alpha}^{d,R}\right), \\ g_n^V &= \left(g_{\alpha\alpha}^{u,L} + g_{\alpha\alpha}^{u,R}\right) + 2\left(g_{\alpha\alpha}^{d,L} + g_{\alpha\alpha}^{d,R}\right), \\ g_p^A &= 2\left(g_{\alpha\alpha}^{u,L} - g_{\alpha\alpha}^{u,R}\right) + \left(g_{\alpha\alpha}^{d,L} - g_{\alpha\alpha}^{d,R}\right), \\ g_n^A &= \left(g_{\alpha\alpha}^{u,L} - g_{\alpha\alpha}^{u,R}\right) + 2\left(g_{\alpha\alpha}^{d,L} - g_{\alpha\alpha}^{d,R}\right). \end{aligned} \tag{16}$$

The axial-vector nucleon form factor takes into account the spin structure of the nucleon and is defined as [56]

$$F_A\left(Q^2\right) = g_A\left(1 + \frac{Q^2}{M_A^2}\right)^{-2}, \tag{17}$$

where $g_A = 1.267$ is the free axial-vector coupling constant and the axial mass is taken to be $M_A = 1$ GeV, while strange quark effects have been neglected.

We note that for spin-zero nuclei the axial-vector contribution vanishes, while for the odd-A nuclei considered in the present study $\mathcal{Q}_W^A$ it is negligible and of the order of $\mathcal{Q}_W^A/\mathcal{Q}_W^V \sim 1/A$. The weak charges in (15) encode crucial information regarding the finite nuclear size through the proton $F_Z^V(Q^2)$ and neutron $F_N^V(Q^2)$ nuclear form factors, which in our work are obtained within the context of the DSM (see below), as functions of the momentum transfer $-q^\mu q_\mu = Q^2 = 2MT_N$. Contrary to similar studies assuming the conventional Helm-type form factors, the present work also takes into account the nuclear effects due to the nonspherical symmetric nuclei employed in dark matter searches.

3.1.2. Electromagnetic Neutrino Contributions. Turning our attention to new physics phenomena we now address potential contributions to CEνNS in the framework of nontrivial neutrino EM interactions that may lead to a new neutrino-floor at low detector thresholds. In this framework, the presence of an effective neutrino magnetic moment μ_ν leads to an EM contribution of the differential cross section that has been written as [41]

$$\left(\frac{d\sigma}{dT_N}\right)_{\mathrm{SM+EM}} = \mathcal{G}_{\mathrm{EM}}\left(E_\nu, T_N\right)\frac{d\sigma_{\mathrm{SM}}}{dT_N}. \tag{18}$$

Neglecting axial effects, the EM contribution to CEνNS at a direct detection dark matter is encoded in the factor

$$\mathcal{G}_{\mathrm{EM}} = 1 + \frac{1}{G_F^2 M}\left(\frac{\mathcal{Q}_{\mathrm{EM}}}{\mathcal{Q}_W^V}\right)^2 \frac{\left(1 - T_N\right)/E_\nu/T_N}{1 - MT_N/2E_\nu^2}, \tag{19}$$

where the relevant EM charge $\mathcal{Q}_{\mathrm{EM}}$ is written in terms of the electron mass m_e, the fine-structure constant a_{EM}, and the effective neutrino magnetic moment as [57]

$$\mathcal{Q}_{\mathrm{EM}} = \frac{\pi a_{\mathrm{EM}}\mu_\nu}{m_e}Z. \tag{20}$$

In contrast to the $\sim N^2$ dependence of the SM case, (19) and (20) imply the existence of a Z^2 coherence along with a characteristic $\sim 1/T_N$ enhancement of the total cross section. This implies a potential distortion of the expected recoil spectrum at very low recoil energies that may be detectable at future direct dark matter detection with sub-keV operation thresholds.

For the sake of completeness, we stress that the effective neutrino magnetic moment μ_ν is expressed through neutrino amplitudes of positive and negative helicity states, e.g., the 3-vectors a_+ and a_- and the neutrino transition magnetic moment matrix, λ, in flavour basis, as [37, 58]

$$\mu_\nu^2 = a_+^\dagger \lambda\lambda^\dagger a_+ + a_-^\dagger \lambda\lambda^\dagger a_-. \tag{21}$$

Then, the effective neutrino magnetic moment is written in mass basis through a proper rotation; for a detailed description of this formalism see [59].

3.1.3. Novel Mediator Contribution. We now explore novel mediator fields that could be accommodated in the context of simplified $U(1)'$ scenarios [60, 61] predicting the existence of a new Z' vector mediator with mass $M_{Z'}$ [62]. Such beyond the SM interactions may constitute a new neutrino-floor at direct detection dark matter experiments [39].

The presence of a Z' mediator gives rise to subleading contributions to the SM CEνNS rate, described by the Lagrangian [63]

$$\mathcal{L}_{\mathrm{vec}} = Z'_\mu\left(g_{Z'}^{qV}\overline{q}\gamma^\mu q + g_{Z'}^{\nu V}\overline{\nu}_L\gamma^\mu\nu_L\right) + \frac{1}{2}M_{Z'}^2 Z'_\mu Z'^\mu, \tag{22}$$

where only left-handed neutrinos are assumed (right-handed neutrinos in the theory would lead to vector-axial-vector cancellations). The resulting cross section reads [41]

$$\left(\frac{d\sigma}{dT_N}\right)_{\mathrm{SM}+Z'} = \mathcal{G}_{Z'}^2\left(Q\right)\frac{d\sigma_{\mathrm{SM}}}{dT_N}, \tag{23}$$

with the factor $\mathcal{G}_{Z'}$ being written in terms of the neutrino-vector coupling $g_{Z'}^{\nu V}$, as

$$\mathcal{G}_{Z'}\left(Q\right) = 1 - \frac{1}{2\sqrt{2}G_F}\frac{\mathcal{Q}_{Z'}}{\mathcal{Q}_W^V}\frac{g_{Z'}^{\nu V}}{Q^2 + M_{Z'}^2}. \tag{24}$$

The relevant charge in this case is expressed through the vector quark couplings $g_{Z'}^{qV}$ to the Z' boson, as [39]

$$\mathcal{Q}_{Z'} = \left(2g_{Z'}^{uV} + g_{Z'}^{dV}\right)Z + \left(g_{Z'}^{uV} + 2g_{Z'}^{dV}\right)N. \tag{25}$$

Let us mention that emerging degeneracies can be either reduced through multidetector measurements [61] or broken in the framework of NSIs [64]. For completeness we note that, despite being not present for the low energies considered here, these couplings could be changed by currently unknown in-medium effects (see, e.g., [23] and references therein).

3.2. Neutrino Sources

3.2.1. Solar Neutrinos. In terrestrial searches for dark matter candidates at low energies, the Solar neutrinos emanating from the interior of the Sun generated through various fusion reactions produce a dominant background for direct CDM detection experiments. Assuming WIMP masses less than 10 GeV, an estimated total Solar neutrino flux of about $6.5 \times 10^{11}\text{cm}^{-2}\text{s}^{-1}$ [65] hitting the Earth is expected to appreciably limit the sensitivity of such experiments [27]. On the other hand, the theoretical uncertainties of Solar neutrinos are presently quite large and depend strongly on the assumed Solar neutrino model. To maintain consistency with existing Solar data, in this work we consider the high metallicity Standard Solar Model (SSM) [21]. We note however that the dominant Solar neutrino component coming from the primary proton-proton channel (*pp* neutrinos) that accounts for about 86% the Solar neutrinos flux has been recently measured by the Borexino experiment with an uncertainty of 1% [66]. Through CEνNS, the direct detection dark matter experiments are mainly sensitive to two sources of Solar neutrinos, namely, the ^{8}B and the *hep* neutrinos which cover the highest energy range of the Solar neutrino spectrum. Since ^{8}B neutrinos are generated from the decay $^8\text{B} \longrightarrow {}^7\text{Be}^* + e^+ + \nu_e$, while *hep* neutrinos from $^3\text{He} + p \longrightarrow {}^4\text{He} + e^+ + \nu_e$, both sources occur in the aftermath of the *pp* chain. Following previous similar studies [28], in this work, we explore the neutrino-floor extending our analysis to the lowest neutrino energies, by considering the *pep* neutrino line which belongs to the *pp* chain and the e^--capture reaction on ^{7}Be that leads to two monochromatic beams at 384.3 and 861.3 keV as well as the well-known CNO cycle. The latter neutrinos appear as three continuous spectra (^{13}N, ^{15}O, and ^{17}F) with end point energies close to the *pep* neutrinos.

3.2.2. Atmospheric Neutrinos. Atmospheric neutrinos are decay products of the particles (mostly pions and kaons) produced as a result of cosmic-ray scattering in the Earth's atmosphere. The generated secondary particles decay to ν_e, $\overline{\nu}_e$, ν_μ, and $\overline{\nu}_\mu$ constituting a significant background to dark matter searches especially for WIMP masses above 100 GeV. In particular, the effect is crucial on the discovery potential of WIMPs with spin-independent cross section of the order of 10^{-48}cm^2. The direct detection dark matter experiments, due to the lack of directional sensitivity, are in principle sensitive to the lowest energy (less than ~100 MeV) atmospheric neutrinos. For this reason, in our present work atmospheric neutrinos are considered by employing the low-energy flux coming out of the FLUKA code simulations [22].

3.2.3. Diffuse Supernova Neutrinos. The weak glow of MeV neutrinos emitted from the total number of core-collapse supernovae, known as the Diffuse Supernova Neutrino Background (DSNB), creates an important source of neutrino background specifically for the WIMPs mass range 10–30 GeV [24]. Despite the appreciably lower flux compared to Solar neutrinos, DSNB neutrino energies are higher than those of the Solar neutrino spectrum. In our simulations, the adopted DSNB distributions (usually of Fermi-Dirac or power-law type) correspond to temperatures 3 MeV for ν_e, 5 MeV for $\overline{\nu}_e$, and 8 MeV for the other neutrino flavours denoted as ν_x or $\overline{\nu}_x$, $x = \mu, \tau$.

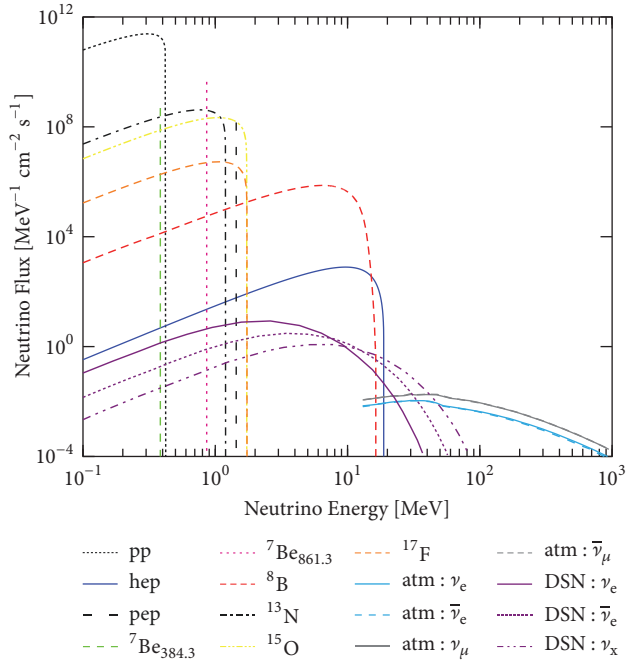

FIGURE 1: Unoscillate neutrino flux considered in the present study, including the Solar, Atmospheric, and DSNB spectra.

Figure 1 shows the unoscillate neutrino flux considered in the present study, illustrating the Solar neutrino spectra of the dominant neutrino sources assuming the high metallicity Standard Solar Model (SSM) as defined in [21]. Also shown is the low-energy atmospheric neutrino flux as obtained from the FLUKA simulation [22] as well as the DSNB spectrum [67]. The corresponding neutrino types, maximum energies, and fluxes are listed in Table 1.

4. Deformed Shell Model

In the formalism of the WIMP-nucleus or neutrino-nucleus event rates of Sections 2 and 3, both for the case of elastic or inelastic interaction channels, the nuclear physics and particle physics (SUSY model) parts appear almost completely separated. In the present work our main focus drops on the nuclear physics aspects which are contained in the nuclear structure factors discussed in Section 2. Special attention is paid on the factors D_i of (9) that depend on the spin structure functions and the nuclear form factors. These quantities have been calculated using the DSM method [48] (for a comprehensive discussion of DSM see [47]) given the kinematics and the assumptions describing the WIMP particles.

The construction of the many-body wave functions for the initial $|J_i^\pi\rangle$ and final $|J_f^\pi\rangle$ nuclear states in the framework of DSM involves performance of the following steps. (i) At first, one chooses a model space consisting of a given set of spherical single-particle (sp) orbits, sp energies, and the

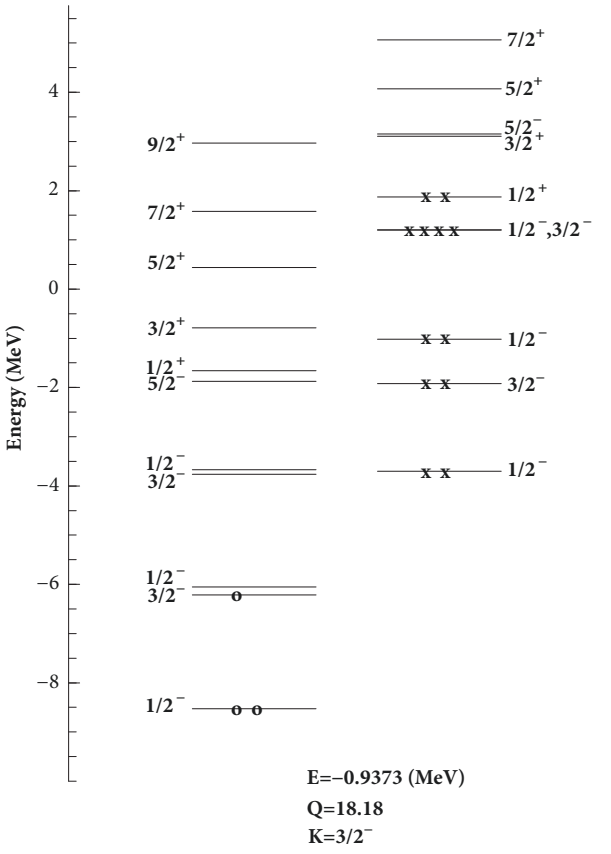

FIGURE 2: HF single-particle spectra for ^{71}Ga corresponding to the lowest prolate configuration. In the figure, circles represent protons and crosses represent neutrons. The HF energy E in MeV, the mass quadrupole moment Q in units of the square of the oscillator length parameter, and the total azimuthal quantum number K are given in the figure.

appropriate two-body effective interaction matrix elements. For ^{71}Ga and ^{75}As, the spherical sp orbits are $1p_{3/2}$, $0f_{5/2}$, $1p_{1/2}$, and $0g_{9/2}$ with energies 0.0, 2.20, 2.28, and 5.40 MeV and 0.0, 0.78, 1.08, and 3.20 MeV, respectively, while the assumed effective interaction is the modified Kuo interaction [68]. Similarly for ^{127}I, the sp orbits, their energies, and the effective interaction are taken from a recent paper [69]. (ii) Assuming axial symmetry and solving the HF single-particle equations self-consistently, the lowest-energy prolate (or oblate) intrinsic state for the nucleus in question is obtained. An example is shown in Figure 2 for ^{71}Ga. (iii) The various excited intrinsic states then are obtained by making particle-hole (p-h) excitations over the lowest-energy intrinsic state (lowest configuration). (iv) Then, because the HF intrinsic nuclear states $|\chi_K(\eta)\rangle$ (K is azimuthal quantum number and η distinguishes states with the same K) do not have definite angular momentum, angular momentum projected states $|\phi^J_{MK}(\mu)\rangle$ are constructed as

$$\left|\phi^J_{MK}(\eta)\right\rangle = \frac{2J+1}{8\pi^2\sqrt{N_{JK}}}\int d\Omega D^{J^*}_{MK}(\Omega)\, R(\Omega)\left|\chi_K(\eta)\right\rangle. \quad (26)$$

In the previous expression, $\Omega = (\alpha, \beta, \gamma)$ represents the Euler angles, $R(\Omega)$ denotes the known general rotation operator, and the Wigner D-matrices are defined as $D^J_{MK}(\Omega) = \langle JM|R(\Omega)|JK\rangle$. Here, N_{JK} is the normalisation constant which by assuming axial symmetry is defined as

$$N_{JK} = \frac{2J+1}{2}\int_0^\pi d\beta \sin\beta d^J_{KK}(\beta)\left\langle\chi_K(\eta)\right| \cdot e^{-i\beta J_y}\left|\chi_K(\eta)\right\rangle, \quad (27)$$

where the functions $d^J_{KK}(\beta)$ are the diagonal elements of the matrix $d^J_{MK}(\beta) = \langle JM|e^{-i\beta J_y}|JK\rangle$. ($v$) Finally, the good angular momentum states ϕ^J_{MK} are orthonormalised by band mixing calculations and then, in terms of the index η, it is possible to distinguish between different states having the same angular momentum J,

$$\left|\Phi^J_M(\eta)\right\rangle = \sum_{K,\alpha} S^J_{K\eta}(\alpha)\left|\phi^J_{MK}(\alpha)\right\rangle. \quad (28)$$

Within the DSM method, for the evaluation of the reduced nuclear matrix element entering (6) and (7), we first calculate the single-particle matrix elements of the relevant operators $t^{(l,s)J}_\nu$, as

$$\begin{aligned}&\left\langle n_i l_i j_i\right|\left|\hat{t}^{(l,s)J}\right|\left|n_k l_k j_k\right\rangle \\ &= \sqrt{(2j_k+1)(2j_i+1)(2J+1)(s+1)(s+2)} \\ &\times \begin{Bmatrix} l_i & \frac{1}{2} & j_i \\ l_k & \frac{1}{2} & j_k \\ l & s & J \end{Bmatrix} \left\langle l_i\right|\left|\sqrt{4\pi}Y^l\right|\left|l_k\right\rangle \left\langle n_i l_i\right| j_l(kr)\left|n_l l_k\right\rangle,\end{aligned} \quad (29)$$

where $\{--\}$ is the 9-j symbol. For more details, the reader is referred to [70–72]. It should be noted that in the DSM method one considers an adequate number of intrinsic states in the band mixing calculations.

DSM calculations are performed in the same spirit as in spherical shell model where one takes a model space and a suitable effective interaction (single-particle orbitals, single-particle energies, and a two-body effective interaction). This procedure has been found to be quite successful in describing the spectroscopic properties and electromagnetic properties of many nuclei in the mass region A = 60–90 and has also been applied to double beta decay nuclear transition matrix elements [47]. In addition, this model has been used recently in calculating the event rates for dark matter detection [48]. With the proper choice of effective interaction, one will not be considering core excitations. This is a standard prescription in shell model as well as in DSM. To go beyond this, one has to use no-core shell model or DSM with much larger set of single-particle orbitals (inclusion of core orbitals), such refinements are planned to be employed in future calculations.

We note that the many-body nuclear calculations performed take into account in the usual way the inert core orbits

Table 2: $2k$ values of the occupied proton and neutron single particle deformed orbits of the HF intrinsic states used in the calculation for each nucleus. The second column gives the serial no. of the HF intrinsic states used. All the $2k$ values are of negative parity unless explicitly shown. The (+), (−), or (±) sign before the $2k$ values implies that either the time-like, time-reversed, or both orbits are occupied. In columns 3 and 4, 3_1 means the first $3/2^-$ HF deformed sp orbit, 3_2 means the second $3/2^-$ deformed HF orbit, and so on (see also Figure 2). Detailed information regarding the structure each of the deformed HF sp orbits, their energies, and the parentage of each of the HF intrinsic state in the Φ^J states (e.g., the linear combination of ϕ^J_{MK} obtained in the band mixing diagonalisation) can be obtained from the authors.

Nucleus	Serial No.	proton orbits			neutron orbits						
^{71}Ga	1	$\pm 1_1$	$+3_1$		$\pm 1_1$	$\pm 1_2$	$\pm 3_1$	$\pm 3_2$	$\pm 1_3$	$\pm 1^+_1$	
	2	$\pm 1_1$	$+1_2$		$\pm 1_1$	$\pm 1_2$	$\pm 3_1$	$\pm 3_2$	$\pm 1_3$	$\pm 1^+_1$	
	3	$\pm 1_1$	-3_1		$\pm 1_1$	$\pm 1_2$	$\pm 3_1$	$\pm 3_2$	$\pm 1_3$	$+1^+$	$+3^+$
	4	$\pm 1_1$	$+3_1$		$\pm 1_1$	$\pm 1_2$	$\pm 3_1$	$\pm 3_2$	$\pm 1_3$	$\pm 5_1$	
^{73}Ge	1	$\pm 1_1$	$\pm 1_2$		$\pm 1_1$	$\pm 1_2$	$\pm 3_1$	$\pm 3_2$	$\pm 1_3$	$\pm 1^+_1$	$+3^+_1$
	2	$\pm 1_1$	$\pm 1_2$		$\pm 1_1$	$\pm 1_2$	$\pm 3_1$	$\pm 3_2$	$\pm 1_3$	$\pm 3^+_1$	$+1^+_1$
	3	$\pm 1_1$	$\pm 3_1$		$\pm 1_1$	$\pm 1_2$	$\pm 3_1$	$\pm 3_2$	$\pm 1_3$	$\pm 1^+_1$	$+3^+_1$
^{75}As	1	$\pm 1_1$	$\pm 1_2$	$+3_1$	$\pm 1_1$	$\pm 1_2$	$\pm 3_1$	$\pm 1^+_1$	$\pm 3^+_1$	$\pm 3_2$	$\pm 1_3$
	2	$\pm 1_1$	$\pm 3_1$	$+1_2$	$\pm 1_1$	$\pm 1_2$	$\pm 3_1$	$\pm 1^+_1$	$\pm 3^+_1$	$\pm 3_2$	$\pm 1_3$
	3	$\pm 1_1$	$\pm 1_2$	$+3_1$	$\pm 1_1$	$\pm 1_2$	$\pm 3_1$	$\pm 1^+_1$	$\pm 3^+_1$	$\pm 3_2$	$\pm 5^+_1$
	4	$\pm 1_1$	$\pm 3_1$	$+1_3$	$\pm 1_1$	$\pm 1_2$	$\pm 3_1$	$\pm 1^+_1$	$\pm 3^+_1$	$\pm 3_2$	$\pm 5^+_1$
	5	$\pm 1_1$	$\pm 1_2$	$+3_1$	$\pm 1_1$	$\pm 1_2$	$\pm 3_1$	$\pm 1^+_1$	$\pm 3^+_1$	$\pm 3_2$	$\pm 5_1$
	6	$\pm 1_1$	$\pm 3_1$	$+1_2$	$\pm 1_1$	$\pm 1_2$	$\pm 3_1$	$\pm 1^+_1$	$\pm 3^+_1$	$\pm 3_2$	$\pm 5_1$
^{127}I	1	$\pm 7^+_1$	$+5^+_1$		$\pm 7^+_1$	$\pm 5^+_1$	$\pm 3^+_1$	$\pm 11_1$	$\pm 1^+_1$	$\pm 5^+_2$	$\pm 9_1$
					$\pm 3^+_2$	$\pm 1^+_2$	$\pm 7_1$	$\pm 5_1$	$\pm 3_1$		
	2	$\pm 7^+_1$	$+5^+_1$		$\pm 7^+_1$	$\pm 5^+_1$	$\pm 3^+_1$	$\pm 11_1$	$\pm 1^+_1$	$\pm 5^+_2$	$\pm 9_1$
					$\pm 3^+_2$	$\pm 1^+_2$	$\pm 7_1$	$\pm 5_1$	$\pm 3^+_3$		
	3	$\pm 7^+_1$	$+3^+_1$		$\pm 7^+_1$	$\pm 5^+_1$	$\pm 3^+_1$	$\pm 11_1$	$\pm 1^+_1$	$\pm 5^+_2$	$\pm 9_1$
					$\pm 3^+_2$	$\pm 1^+_2$	$\pm 7_1$	$\pm 5_1$	$\pm 3_1$		
	4	$\pm 7^+_1$	$+3^+_1$		$\pm 7^+_1$	$\pm 5^+_1$	$\pm 3^+_1$	$\pm 11_1$	$\pm 1^+_1$	$\pm 5^+_2$	$\pm 9_1$
					$\pm 3^+_2$	$\pm 1^+_2$	$\pm 7_1$	$\pm 5_1$	$\pm 3^+_3$		
	5	$\pm 7^+_1$	$+1^+_1$		$\pm 7^+_1$	$\pm 5^+_1$	$\pm 3^+_1$	$\pm 11_1$	$\pm 1^+_1$	$\pm 5^+_2$	$\pm 9_1$
					$\pm 3^+_2$	$\pm 1^+_2$	$\pm 7_1$	$\pm 5_1$	$\pm 3_1$		
	6	$\pm 7^+_1$	$+1^+_1$		$\pm 7^+_1$	$\pm 5^+_1$	$\pm 3^+_1$	$\pm 11_1$	$\pm 1^+_1$	$\pm 5^+_2$	$\pm 9_1$
					$\pm 3^+_2$	$\pm 1^+_2$	$\pm 7_1$	$\pm 5_1$	$\pm 3^+_3$		

(completely filled by the protons and neutrons) and the extra-core nucleons moving in the assumed model space under the influence of an effective interaction. The explicit $2k$ values of the occupied nucleon single-particle deformed orbits of the HF intrinsic states considered in our calculations are listed in Table 2.

5. Results and Discussion

5.1. Nuclear Physics Aspects. To maximise the significance of our WIMP-nucleus and neutrino-floor calculations, the reliability of the obtained nuclear wave functions is tested by comparing the extracted energy level spectrum and magnetic moments with available experimental data. The consistency of this method obtained for ^{73}Ge has been already presented in [48]. Furthermore, in the DSM calculations for ^{71}Ga and ^{75}As, we restrict ourselves to prolate solutions only, since the oblate solution does not reproduce the energy spectra and electromagnetic properties of these nuclei. It also does not mix with the prolate solution. Hence, we neglect the oblate solutions in the calculations. For each of these nuclei, we consider only four intrinsic prolate states which should be sufficient to explain the systematics of the ground state and close lying excited state. Due to size restrictions, in Figure 3 we illustrate only the calculated spectrum for ^{71}Ga.

For ^{75}As, the ground state is $3/2^-$ and there are also two $1/2^-$ and $3/2^-$ levels around 0.12 MeV. In addition, there is a collective band consisting of $5/2^-$, $9/2^-$, and $13/2^-$ $17/2^-$ levels at 0.279, 1.095, 2.150, and 3.091 MeV, respectively. All these levels are well reproduced by the DSM method. Turning to the ^{127}I spectrum, there are four observed collective bands with band heads $5/2^+$, $(7/2^+)_{1,2}$, and $9/2^+$. There are evidences suggesting that low-lying states in ^{127}I have oblate deformation [73]. Hence, for this nucleus, we consider only oblate configurations and take the six lowest oblate intrinsic states in the band mixing calculation. These intrinsic states are found to provide adequate description of the energy spectrum and electromagnetic properties for this nucleus. The calculations for this nucleus utilise a new effective interaction developed by an Italian group very recently [69]. The new effective interaction is seen to reproduce well the ^{127}I spectrum; details will be presented elsewhere.

We thus conclude that concerning the evaluation of the WIMP-nucleus and CEνNS event rates we are interested in

Table 3: List of potential dark matter detectors considered in the present study. The calculated magnetic moments for the ground states of ^{71}Ga, ^{73}Ge, ^{75}As, and ^{127}I are shown. The results involve the bare gyromagnetic ratios and experimental data are from [44]. The ground state J^π and the harmonic oscillator size b are also shown.

Nucleus	A	Z	J^π	$< l_p >$	$< S_p >$	$< l_n >$	$< S_n >$	μ (nm)	Exp	b [fm^{-1}]
Ga	71	31	$3/2^-$	0.863	0.257	0.369	0.011	2.259	2.562	1.90
Ge	73	32	$9/2^+$	0.581	−0.001	3.558	0.362	−0.811	−0.879	1.91
As	75	33	$(3/2^-)_1$	0.667	0.164	0.626	0.042	1.422	1.439	1.92
I	127	53	$5/2^+$	2.395	−0.211	0.313	2.343	1.207	2.813	2.09

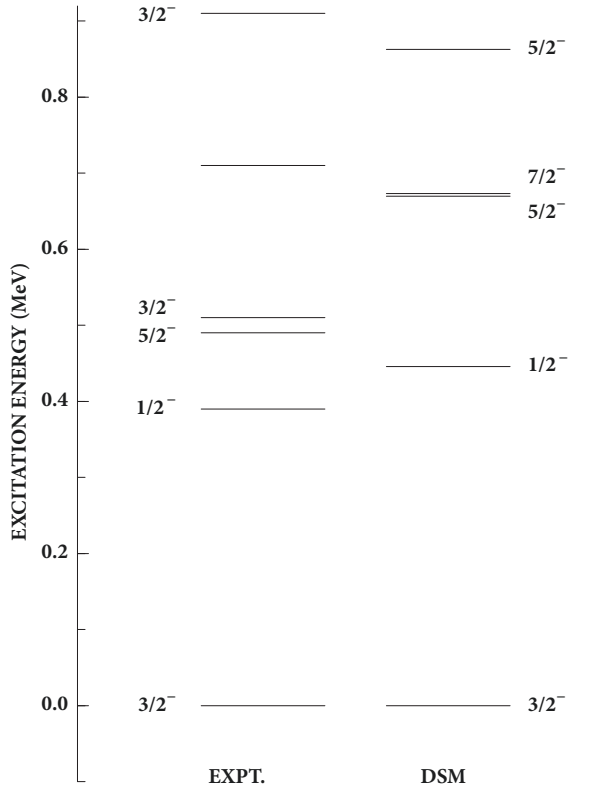

Figure 3: Comparison of deformed shell model results with experimental data for ^{71}Ga for low-lying states. The experimental values are taken from [44].

this work, the required ground state wave functions obtained through the DSM method are reliable and the intrinsic states used in the subsequent analysis are considered sufficient. From the perspective of nuclear physics, spin contributions constitute significant ingredients in the evaluation of WIMP-nucleus event rates. For this reason, the first stage of our work involves the calculation of the magnetic moment, which is decomposed into an orbital and spin part. The relevant results for the proton and neutron contributions to the orbital and spin parts concerning the ground states of the four nuclear isotopes studied in this paper are given in Table 3. A comparison between the obtained magnetic moments and the respective experimental data is also provided. Despite the fact that these calculations adopt bare values of g-factors neglecting quenching effects, the obtained DSM results of the ground state magnetic moments are consistent with the experimental values.

Having successfully reproduced the energy spectrum and the magnetic moments within the context of the DSM wave functions, we evaluate important nuclear physics inputs entering the WIMP-nucleus and CEνNS cross sections. Figures 4 and 5 present a comparison between the DSM nuclear form factors and the effective Helm-type ones employed in various similar studies, where, as can be seen, the DSM results differ from the Helm-type ones. The behaviour of the proton form factor for ^{71}Ga is found to be different from those of the other nuclei and this may be due to the nearby proton shell closure and the neutron subshell closure. Calculations with several different effective interactions are under way to rule out the possibility of any deficiency of the effective two-body interaction used. We furthermore illustrate the spin structure functions of WIMP-^{71}Ga elastic scattering calculated using (6) and (7). The variation of F_{00}, F_{01}, and F_{11} with respect to the parameter u is shown in Figure 6, while similar results are obtained for ^{75}As and ^{127}I (for the ^{73}Ge case see [48]).

The consistency of our nuclear physics DSM calculations has been extensively explored in this work and compared with existing experimental data (see Figures 2 and 3 and Table 3) making the considered form factors reliable. Specifically we have tested the reliability of this model to describe nuclear structure properties such as excitation spectra and nuclear magnetic moments. We mention that DSM has been tested in the past in many nuclei in the A = 60–90 region [47] (see above).

5.2. WIMP-Nucleus Rates and the Neutrino-Floor. The WIMP-nucleus event rates and the neutrino-floor due to neutrino-nucleus scattering are calculated for a set of interesting nuclear targets such as ^{71}Ga, ^{73}Ge, ^{75}As, and ^{127}I (see Table 3). In evaluating the neutrino-induced backgrounds, we consider only the dominant CEνNS channel, since neutrino-electron events are expected to produce less events by about one order of magnitude [27]. For the case of a ^{71}Ga target, in Figure 7 we provide the coefficients D_i associated with the spin dependent and coherent interactions given in (9) as functions of the WIMP mass m_χ by assuming three typical values of the detector threshold energy T_N= 0, 5, 10 keV. For the special case of T_N = 0, all plots peak at m_χ ~35 GeV, while for higher threshold energies D_i are shifted towards higher values of the WIMP mass. The calculations take also into account the annual modulation which is represented by the curve thickness. As can be seen from the figure, the modulation signal varies with respect to the WIMP mass, being larger for $m_\chi \leq 50$ GeV, while its magnitude is slightly different for the spin dependent and coherent channels.

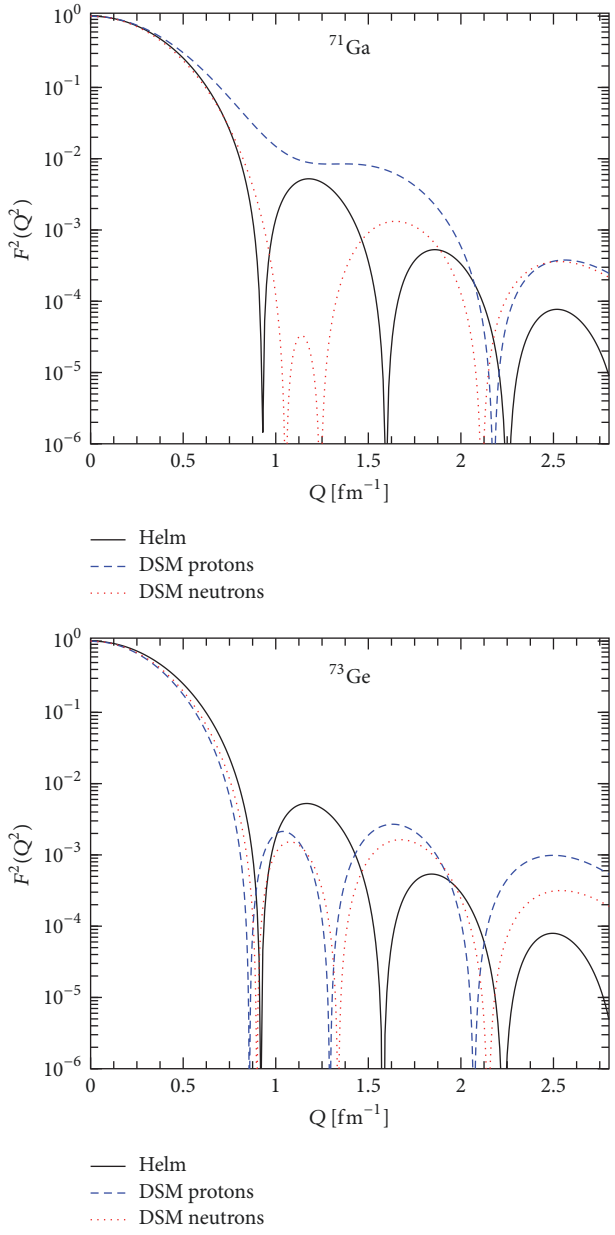

FIGURE 4: Comparison of the DSM nuclear form factors of the ^{71}Ga and ^{73}Ge isotopes, obtained in the present work with the corresponding effective Helm form factors.

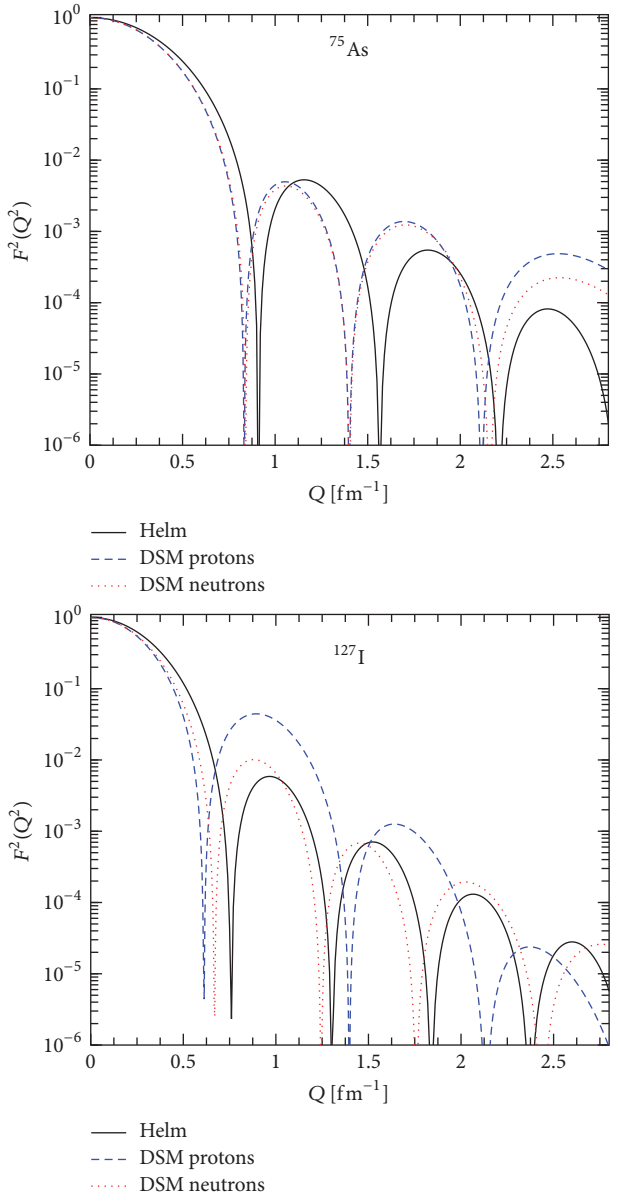

FIGURE 5: Same as in Figure 4 but for the ^{75}As and ^{127}I isotopes.

Proceeding further, in Figure 8 we evaluate the expected event rates for the four target nuclei assuming elastic WIMP scattering for WIMP candidates with mass $m_\chi = 110$ GeV, by adopting the nucleonic-current parameters $f_A^0 = 3.55 \times 10^{-2}$, $f_A^1 = 5.31 \times 10^{-2}$, $f_S^0 = 8.02 \times 10^{-4}$, and $f_S^1 = -0.15 \times f_S^0$. As in the previous discussion, the thickness of the graph accounts for the annual modulation. We find that there is a strong dependence of the event rate on the studied nuclear isotope. Again the modulation is found to decrease for heavier mass. Among the four studied nuclei, we come out with a larger event rate for the case of a ^{71}Ga nuclear detector, since D_1, D_2, and D_3 are all positive and have similar values. For ^{73}Ge, D_2 is negative and its magnitude is comparable to D_1 and D_3, while for ^{75}As, D_3 is positive but small, and finally for ^{127}I, D_2 and D_3 are relatively smaller and D_1 is large. The coherent contribution D_4 has more or less similar values for all nuclei considered.

For each component of the Solar, Atmospheric, and DSNB neutrino distributions we calculate the expected neutrino-floor due to CEνNS, by considering the target nuclei presented in Table 3. In our calculations, we neglect possible recoil events arising from Geoneutrinos as they are expected to be at least one order of magnitude less that the aforementioned neutrino sources (see, e.g., [25, 26]). In order to make a quantitative estimate of the neutrino-floor, here we do not consider neutrino oscillations and we assume that CEνNS is a flavour blind process in the SM. The

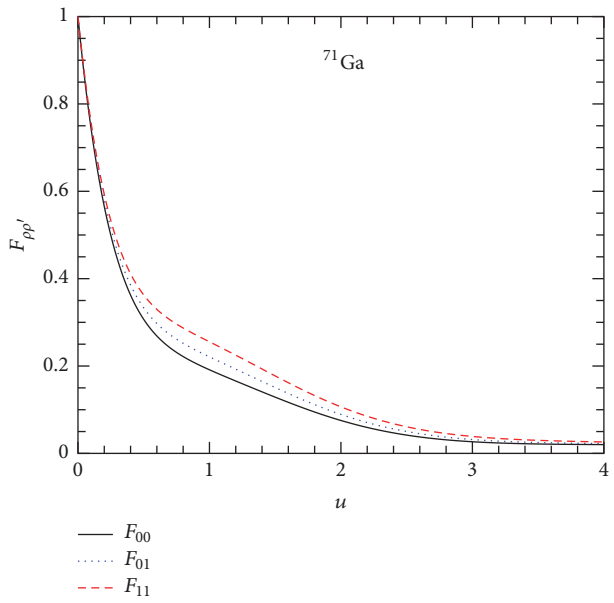

FIGURE 6: Normalised spin structure functions of ^{71}Ga for the ground state.

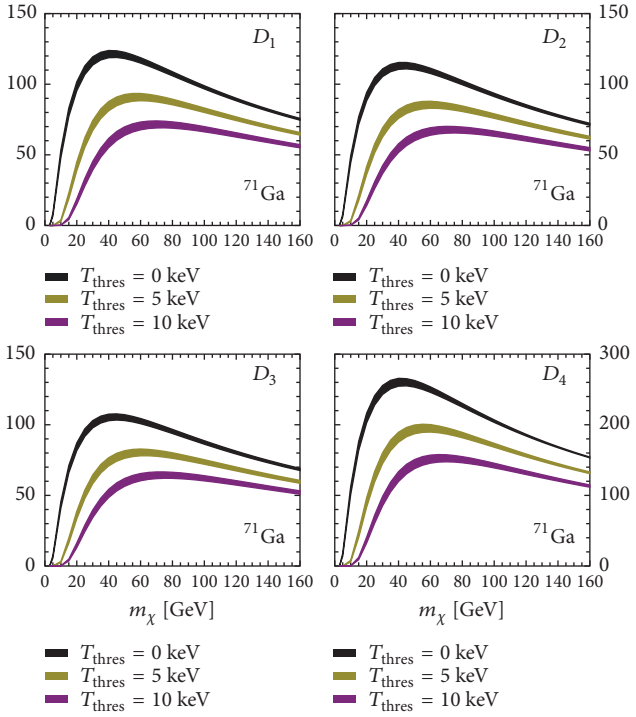

FIGURE 7: Nuclear structure coefficients D_i for ^{71}Ga plotted as a function of the WIMP mass. The graphs are plotted for three values of the detector threshold 0, 5, and 10 keV. The thickness of the graphs represents annual modulation.

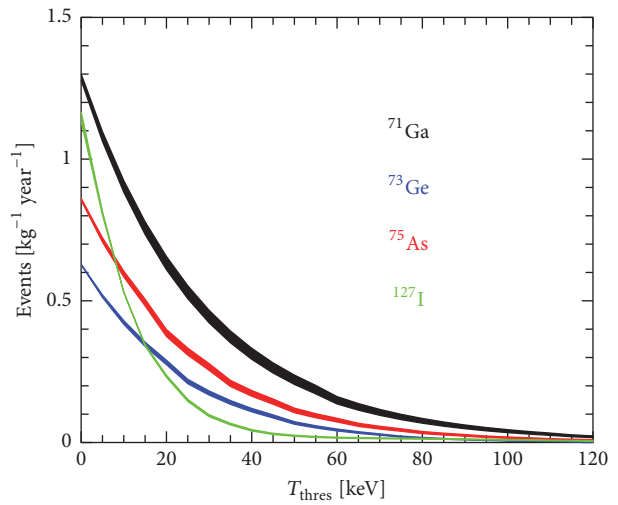

FIGURE 8: The WIMP event rates for ^{71}Ga, ^{73}Ge, ^{75}As, and ^{127}I detectors in units of kg^{-1} year^{-1} as a function of the detector threshold T_N. The nuclear threshold T_N energy through the limit of the integration in (9). The thickness of the curve represents the annual modulation which decreases with increasing nuclear mass.

differential event rate due to CEνNS, for the various dark matter detectors considered in the present study, is presented in Figure 9. It can be noticed that the neutrino background is dominated by Solar neutrinos at very low recoil energies. We stress that, for the typical keV-recoil thresholds of the current direct detection dark matter experiments only the *hep* and ^{8}B sources constitute a possibly detectable background. From our results we conclude that, for recoil energies above about 10 keV, Atmospheric neutrinos dominate the neutrino background event rates, having a tiny contribution coming from the DSNB spectrum.

The number of expected background events due to CEνNS for each component of the Solar, Atmospheric, and DSNB neutrino fluxes is illustrated in Figure 10. Similar to the differential event case, at low energies the neutrino background is dominated by the Solar neutrino spectrum with the dominant components being the *hep* and ^{8}B neutrino sources. The results imply that future multi-ton scale detectors with sub-keV sensitivities may be also sensitive to ^{7}Be and *pp* neutrinos. We comment however that such sensitivities will be further limited due to the quenching effect of the nuclear recoil spectrum which is not taken into account here. Moreover, it is worth mentioning that neutrino-induced and WIMP-nucleus scattering processes provide similar recoil spectra; e.g., the recoil spectrum of ^{8}B neutrinos may mimic that of a WIMP with mass 6 GeV (100 MeV) [28].

At this point, we consider additional interactions in the context of new physics beyond the SM that may enhance the CEνNS rate at a direct detection dark matter experiment. Specifically we study the impact of neutrino EM properties as well as the impact of new interactions due to a Z' mediator, on the neutrino floor. In our calculations we assume the existence of a neutrino magnetic moment $\mu_\nu = 4.3 \times 10^{-9}\mu_B$, extracted from CE$\nu$NS data in [41] as well as the corresponding limit from $\overline{\nu}_e - e^-$ scattering data of the GEMMA experiment, e.g., $\mu_{\overline{\nu}_e} = 2.9{\times}10^{-11}\mu_B$ [74]. Regarding the Z' interaction we consider typical values such as $M'_Z = 10$ MeV, $g^2_{Z'} = 10^{-6}$, and $M'_Z = 1$GeV, $g^2_{Z'} = 10^{-6}$

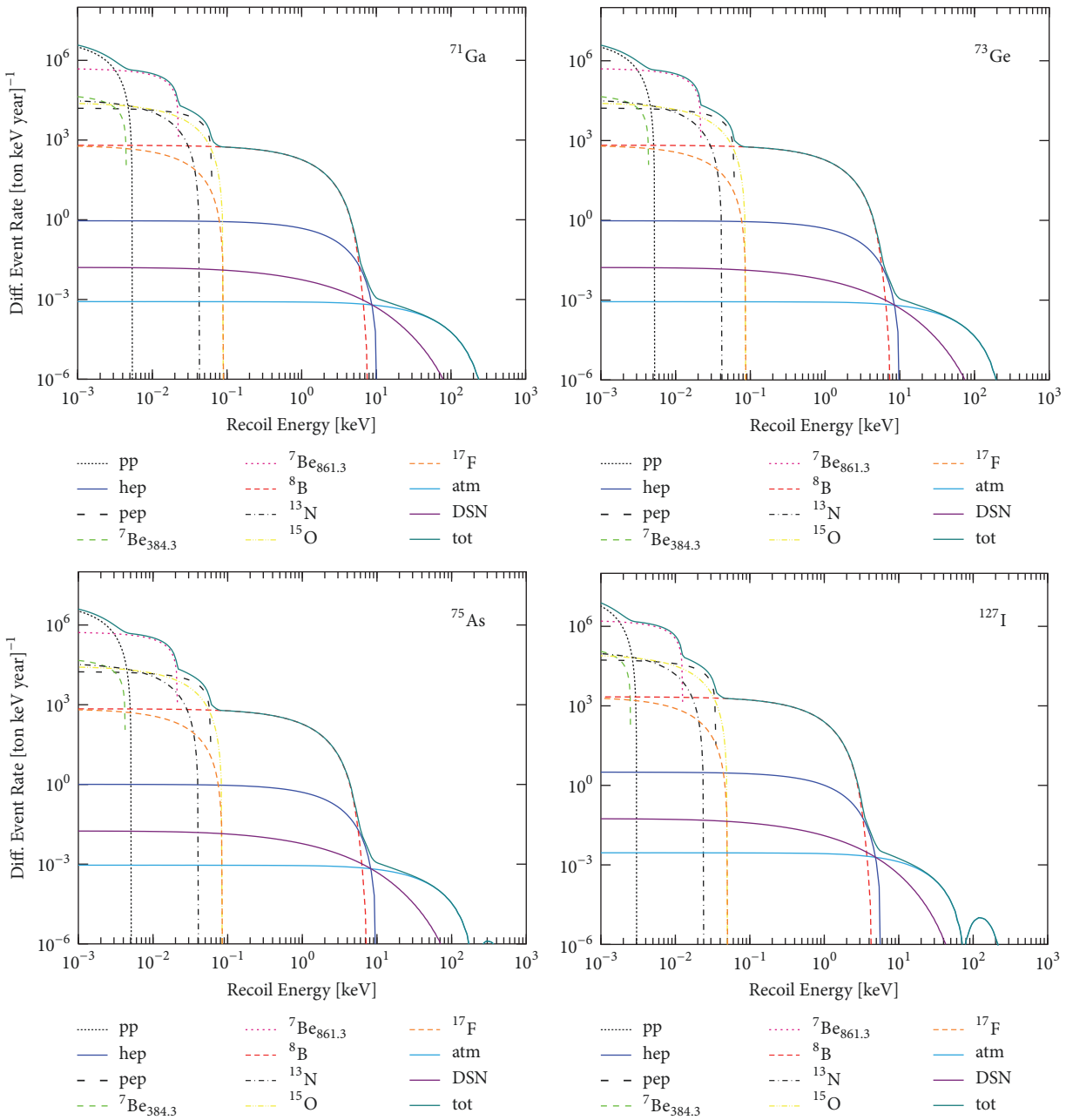

FIGURE 9: Differential event rate of the neutrino-floor assuming ^{71}Ga, ^{73}Ge, ^{75}As, and ^{127}I as cold dark matter detectors. The individual components coming from the Solar, Atmospheric, and DSNB flux are also shown.

[75]. Following [64], by assuming universal couplings, our calculations involve the product of neutrino and quark Z' couplings defined as (for a comprehensive study involving the flavour dependence of the Z' couplings the reader is refereed to [76])

$$g_{Z'}^2 = \frac{g_{Z'}^{\nu V} \mathcal{Q}_{Z'}}{3A}. \tag{30}$$

The corresponding results are presented in Figure 11, indicating that such new physics phenomena may constitute a crucial source of background even for multi-ton scale detectors with sub-keV capabilities. We stress, however, that the latter conclusion depends largely on the assumed parameters, which currently are unknown.

Before closing, we estimate the difference in the calculated number of neutrino-floor events between the conventional Helm-type and DSM predictions by defining the ratio

$$\mathcal{R} = \frac{\text{DSM}_{\text{events}}}{\text{Helm}_{\text{events}}}. \tag{31}$$

For each nuclear system, the corresponding results are presented in Figure 12 indicating that the differences can become significant, especially in the high energy tail of the detected recoil spectrum.

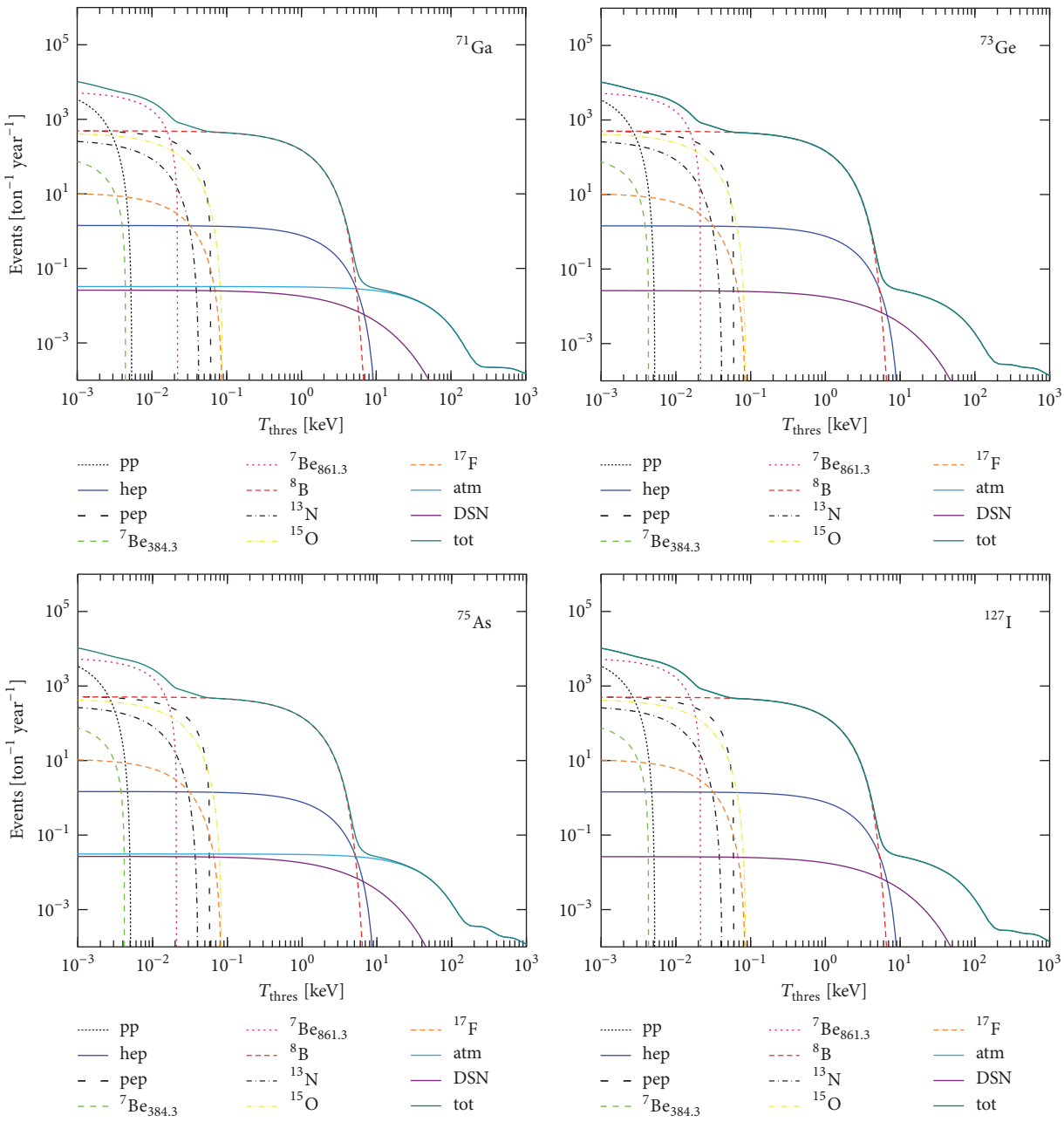

FIGURE 10: Same as in Figure 9 but for the number of events above the detector threshold.

6. Conclusions

In this work, we studied comprehensively the expected event rates in WIMP-nucleus and neutrino-floor processes by performing reliable calculations for a set of prominent nuclear materials of direct dark matter detection experiments. The detailed calculations involve crucial nuclear physics inputs in the framework of the deformed shell model based on Hartree-Fock nuclear states. This way, the nuclear deformation and the spin structure effects of odd-A isotopes that play significant role in searching for dark matter candidates are incorporated. The chosen nuclear detectors involve popular nuclear isotopes in dark matter investigations such as the ^{71}Ga, ^{73}Ge, ^{75}As, and ^{127}I isotopes. The DSM results indicate that ^{71}Ga needs further investigation by employing another effective two-body interaction than the one used in the chosen set of nuclear isotopes.

The deformed shell model (DSM) employed for the nuclear structure calculations in this work is very well tested in many examples in the past [47] for nuclei with A=60–90. Therefore, in our study we have chosen the dark matter candidates ^{71}Ga, ^{73}Ge, and ^{75}As. In addition, to extend DSM to heavier nuclei of interest in dark matter detection, we have considered ^{127}I and the results, reported in the present paper, are quite encouraging. In the near future we will consider Xe isotopes that are also of current interest. For lighter candidate

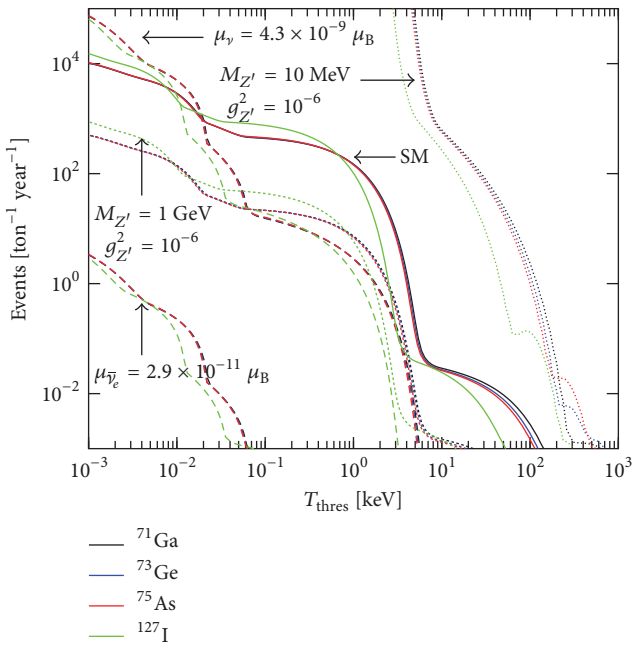

Figure 11: The neutrino-floor for various interaction channels. Solid, dashed, and dotted lines correspond to SM, EM, and Z' contributions, respectively.

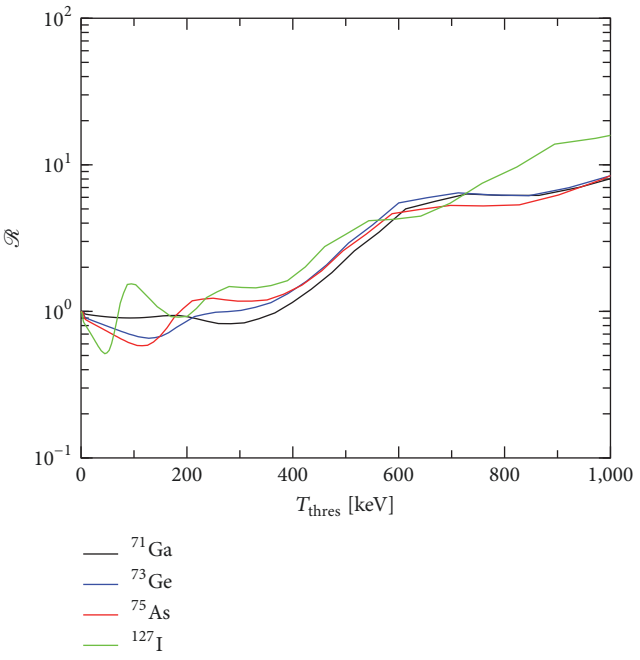

Figure 12: The ratio $\mathscr{R}$ as a function of the detector threshold.

nuclei, such as Na, Si, and Ar, clearly shell model will be better choice and DSM may also be tested for these isotopes.

More importantly, by exploiting the expected neutrino-floor due to Solar, Atmospheric, and DSNB neutrinos, which constitute an important source of background to dark matter searches, the impacts of new physics CEνNS contributions based on novel electromagnetic neutrino properties and Z' mediator bosons have been estimated and discussed. Our results also indicate that the addressed novel contributions may lead to a distortion of the expected recoil spectrum that could limit the sensitivity of upcoming WIMP searches. Such aspects could also provide key information concerning existing anomalies in B-meson decay at the LHCb experiment [77] and offer new insights into the LMA-Dark solution [78, 79].

Finally, the present results indicate that the addressed nuclear effects may become significant, leading to alterations especially in the high energy tail of the expected neutrino-floor as described by effective nuclear calculations, thus motivating further studies in the context of advanced nuclear physics methods such as the deformed shell model or the Quasiparticle Random Phase approximations and others. Such a comprehensive study using available data of the COHERENT experiment is under way and will be presented elsewhere.

Data Availability

The data used to support the findings of this study are available from the corresponding author upon request.

Conflicts of Interest

The authors declare that they have no conflicts of interest.

Acknowledgments

R. Sahu is thankful to SERB of Department of Science and Technology (Government of India) for financial support. D. K. Papoulias is grateful to Professor Naumov for stimulating discussions.

References

[1] G. Jungman, M. Kamionkowski, and K. Griest, "Supersymmetric dark matter," *Physics Reports*, vol. 267, no. 5-6, pp. 195–373, 1996.

[2] G. Hinshaw, D. Larson, E. Komatsu et al., "Nine-Year Wilkinson Microwave Anisotropy Probe (WMAP) Observations: Cosmological Parameter Results," *The Astrophysical Journal Supplement Series*, vol. 208, p. 19, 2013.

[3] G. F. Smoot, C. L. Bennett, and A. Kogut, "Structure in the COBE differential microwave radiometer first-year maps," *The Astrophysical Journal* , vol. 396, no. 1, pp. L1–L5, 1992.

[4] P. A. R. Ade, N. Aghanim, M. Arnaud et al., "Planck 2015 results. XIII. Cosmological parameters," *Astronomy & Astrophysics*, vol. A13, p. 594, 2016.

[5] S. Das, T. Louis, M. R. Nolta et al., "The Atacama Cosmology Telescope: Temperature and Gravitational Lensing Power Spectrum Measurements from Three Seasons of Data," *Journal of Cosmology and Astroparticle Physics*, vol. 2014, no. 04, p. 14, 2014.

[6] E. M. George, C. L. Reichardt, K. A. Aird et al., "A measurement of secondary cosmic microwave background anisotropies from the 2500-square-degree SPT-SZ survey," *The Astrophysical Journal*, vol. 799, p. 177, 2015, https://arxiv.org/abs/1408.3161.

[7] E. Gawiser, "Extracting Primordial Density Fluctuations," *Science*, vol. 280, no. 5368, pp. 1405–1411.

[8] T. S. Kosmas and J. D. Vergados, "Cold dark matter in SUSY theories: the role of nuclear form factors and the folding with the LSP velocity," *Physical Review D: Particles, Fields, Gravitation and Cosmology*, vol. 55, no. 4, pp. 1752–1764, 1997.

[9] G. Bertone, D. Hooper, and J. Silk, "Particle dark matter: evidence, candidates and constraints," *Physics Reports*, vol. 405, no. 5-6, pp. 279–390, 2005.

[10] M. Kortelainen, T. Kosmas, J. Suhonen, and J. Toivanen, "Event rates for CDM detectors from large-scale shell-model calculations," *Physics Letters B*, vol. 632, no. 2-3, pp. 226–232, 2006.

[11] J. L. Feng, "Dark Matter Candidates from Particle Physics and Methods of Detection," *Annual Review of Astronomy and Astrophysics*, vol. 48, p. 495, 2010, https://arxiv.org/abs/1003.0904.

[12] A. L. Fitzpatrick, W. Haxton, E. Katz, N. Lubbers, and Y. Xu, "The effective field theory of dark matter direct detection," *Journal of Cosmology and Astroparticle Physics*, vol. 2013, no. 02, pp. 004-004, 2013.

[13] J. Vergados, F. Avignone, P. Pirinen, P. Srivastava, M. Kortelainen, and J. Suhonen, " Theoretical direct WIMP detection rates for transitions to the first excited state in ," *Physical Review D: Particles, Fields, Gravitation and Cosmology*, vol. 92, no. 1, 2015.

[14] P. C. Divari, T. S. Kosmas, J. D. Vergados, and L. D. Skouras, "Shell model calculations for light supersymmetric particle scattering off light nuclei," *Physical Review C: Nuclear Physics*, vol. 61, no. 5, 2000.

[15] E. Holmlund, M. Kortelainen, T. S. Kosmas, J. Suhonen, and J. Toivanen, "Microscopic calculation of the LSP detection rates for the ^{71}Ga, ^{73}Ge and ^{127}I dark-matter detectors," *Physics Letters B*, vol. 584, no. 1-2, pp. 31–39, 2004.

[16] D. S. Akerib and CDMS Collaboration, "Exclusion Limits on the WIMP-Nucleon Cross-Section from the First Run of the Cryogenic Dark Matter Search in the Soudan Underground Lab," *Physical Review D*, vol. 72, Article ID 052009, 2005, https://arxiv.org/abs/astro-ph/0507190.

[17] A. Broniatowski and EDELWEISS Collaboration, "A new high-background-rejection dark matter Ge cryogenic detector," *Physics Letters B*, vol. 681, no. 4, pp. 305–309, 2009.

[18] K. Freese, M. Lisanti, and C. Savage, "Annual Modulation of Dark Matter: A Review," *Reviews of Modern Physics*, vol. 85, no. 4, pp. 1561–1581, 2013.

[19] D. S. Akerib, S. Alsum, H. M. Araújo et al., "Results from a search for dark matter in the complete LUX exposure," *Physical Review Letters*, vol. 118, Article ID 021303, 2017, https://arxiv.org/abs/1608.07648.

[20] C. Fu and PandaX-II Collaboration, "Spin-Dependent Weakly-Interacting-Massive-Particle–Nucleon Cross Section Limits from First Data of PandaX-II Experiment," *Physical Review Letters*, vol. 118, Article ID 071301, 2017, [Erratum: *Physical Review Letters*, vol. 120, no.4, Article ID 049902, 2018].

[21] W. C. Haxton, R. G. Hamish Robertson, and A. M. Serenelli, "Solar Neutrinos: Status and Prospects," *Annual Review of Astronomy and Astrophysics*, vol. 51, p. 21, 2013, https://arxiv.org/abs/1208.5723.

[22] G. Battistoni, A. Ferrari, T. Montaruli, and P. R. Sala, "The atmospheric neutrino flux below 100 MeV: The FLUKA results," *Astroparticle Physics*, vol. 23, no. 5, pp. 526–534, 2005.

[23] K. C. Y. Ng, J. F. Beacom, A. H. G. Peter, and C. Rott, "Solar atmospheric neutrinos: A new neutrino floor for dark matter searches," *Physical Review D: Particles, Fields, Gravitation and Cosmology*, vol. 96, Article ID 103006, 2017.

[24] J. F. Beacom, "The Diffuse Supernova Neutrino Background," *Annual Review of Nuclear and Particle Science*, vol. 60, pp. 439–462, 2010.

[25] J. Monroe and P. Fisher, "Neutrino backgrounds to dark matter searches," *Physical Review D*, vol. 76, Article ID 033007, 2007.

[26] G. B. Gelmini, V. Takhistov, and S. J. Witte, "Casting a wide signal net with future direct dark matter detection experiments," *Journal of Cosmology and Astroparticle Physics*, 2018.

[27] J. Billard, E. Figueroa-Feliciano, and L. Strigari, "Implication of neutrino backgrounds on the reach of next generation dark matter direct detection experiments," *Physical Review D: Particles, Fields, Gravitation and Cosmology*, vol. 89, no. 2, Article ID 023524, 2014.

[28] C. A. O'Hare, "Dark matter astrophysical uncertainties and the neutrino floor," *Physical Review D*, vol. 94, Article ID 063527, 2016.

[29] J. B. R. Battat et al., "Readout technologies for directional WIMP Dark Matter detection," *Physics Reports*, vol. 662, pp. 1–46, 2016.

[30] D. Z. Freedman, "Coherent effects of a weak neutral current," *Physical Review D: Particles, Fields, Gravitation and Cosmology*, vol. 9, no. 5, pp. 1389–1392, 1974.

[31] V. A. Bednyakov and D. V. Naumov, "Coherency and incoherency in neutrino-nucleus elastic and inelastic scattering," https://arxiv.org/abs/1806.08768.

[32] D. Akimov et al., "Observation of coherent elastic neutrino-nucleus scattering," *Science*, vol. 357, pp. 1123–1126, 2017.

[33] D. K. Papoulias and T. S. Kosmas, "Nuclear aspects of neutral current non-standard ν-nucleus reactions and the role of the exotic $\mu^- \longrightarrow e^-$ transitions experimental limits," *Physics Letters B*, vol. 728, p. 482, 2014.

[34] P. Coloma, M. C. Gonzalez-Garcia, M. Maltoni, and T. Schwetz, "A COHERENT enlightenment of the neutrino Dark Side," *Physical Review D*, vol. 96, Article ID 115007, 2017.

[35] D. Aristizabal Sierra, N. Rojas, and M. H. G. Tytgat, "Neutrino non-standard interactions and dark matter searches with multi-ton scale detectors," https://arxiv.org/abs/1712.09667.

[36] D. Papoulias and T. Kosmas, "Standard and Nonstandard Neutrino-Nucleus Reactions Cross Sections and Event Rates to Neutrino Detection Experiments," *Advances in High Energy Physics*, vol. 2015, Article ID 763648, 17 pages, 2015.

[37] T. S. Kosmas, O. G. Miranda, D. K. Papoulias, M. Tortola, and J. W. F. Valle, "Probing neutrino magnetic moments at the Spallation Neutron Source facility," *Physical Review D*, vol. 92, Article ID 013011, 2015.

[38] T. S. Kosmas, O. G. Miranda, D. K. Papoulias, M. Tortola, and J. W. F. Valle, "Sensitivities to neutrino electromagnetic properties at the TEXONO experiment," *Physics Letters B*, vol. 750, p. 459, 2015.

[39] E. Bertuzzo, F. F. Deppisch, S. Kulkarni, Y. F. Perez Gonzalez, and R. Z. Funchal, "Dark matter and exotic neutrino interactions in direct detection searches," *Journal of High Energy Physics*, vol. 2017, no. 4, 2017.

[40] J. B. Dent, B. Dutta, J. L. Newstead, and L. E. Strigari, "Dark matter, light mediators, and the neutrino floor," *Physical Review D: Particles, Fields, Gravitation and Cosmology*, vol. 95, no. 5, 2017.

[41] D. Papoulias and T. Kosmas, "COHERENT constraints to conventional and exotic neutrino physics," *Physical Review D: Particles, Fields, Gravitation and Cosmology*, vol. 97, no. 3, 2018.

[42] A. Cisterna, T. Delsate, L. Ducobu, and M. Rinaldi, "Sensitivity to Z-prime and nonstandard neutrino interactions from ultralow threshold neutrino-nucleus coherent scattering," *Physical Review D*, vol. 93, Article ID 013015, 2016.

[43] L. E. Strigari, "Neutrino floor at ultralow threshold," *Physical Review D*, vol. 93, Article ID 103534, 2016.

[44] http://www.nndc.bnl.gov/ensdf.

[45] S. Gardner and G. Fuller, "Dark matter studies entrain nuclear physics," *Progress in Particle and Nuclear Physics*, vol. 71, pp. 167–184, 2013.

[46] T. S. Kosmas, A. Faessler, and R. Sahu, " Transition matrix elements for ," *Physical Review C: Nuclear Physics*, vol. 68, no. 5, 2003.

[47] V. K. B. Kota and R. Sahu, *Structure of Medium Mass Nuclei: Deformed Shell Model and Spin-Isospin Interact-ing Boson Model*, CRC Press, 2016.

[48] R. Sahu and V. K. Kota, "Deformed shell model study of event rates for WIMP-73Ge scattering," *Modern Physics Letters A*, vol. 32, no. 38, p. 1750210, 2017.

[49] P. Pirinen, P. Srivastava, J. Suhonen, and M. Kortelainen, " Shell-model study on event rates of lightest supersymmetric particles scattering off ," *Physical Review D: Particles, Fields, Gravitation and Cosmology*, vol. 93, no. 9, 2016.

[50] P. Toivanen, M. Kortelainen, J. Suhonen, and J. Toivanen, "Large-scale shell-model calculations of elastic and inelastic scattering rates of lightest supersymmetric particles (LSP) on I-127, Xe-129, Xe-131, and Cs-133 nuclei," *Physical Review C*, vol. 79, Article ID 044302, 2009.

[51] J. D. Vergados and T. S. Kosmas, "Searching for Cold Dark Matter. A case of coexistence of Supersymmetry and Nuclear Physics," *Physics of Atomic Nuclei*, vol. 61, p. 1066, 1998, https://arxiv.org/abs/hep-ph/9802270.

[52] J. Wyenberg and I. M. Shoemaker, "Mapping The Neutrino Floor For Dark Matter-Electron Direct Detection Experiments," *Physical Review D*, vol. 79, Article ID 115026, 2018.

[53] D. K. Papoulias and T. S. Kosmas, "Neutrino transition magnetic moments within the non-standard neutrino-nucleus interactions," *Physics Letters B*, vol. 747, pp. 454–459, 2015.

[54] J. Beringer, J. F. Arguin, and R. M. Barnett, "Review of particle physics," *Physical Review D: Particles, Fields, Gravitation and Cosmology*, vol. 86, no. 1, Article ID 010001, 2012.

[55] J. Barranco, O. G. Miranda, and T. I. Rashba, "Probing new physics with coherent neutrino scattering off nuclei," *Journal of High Energy Physics*, vol. 2005, article 021, 14 pages, 2005.

[56] W. M. Alberico, S. M. Bilenky, and C. Maieron, "Strangeness in the nucleon: neutrino—nucleon and polarized electron—nucleon scattering," *Physics Reports*, vol. 358, no. 4, pp. 227–308, 2002.

[57] K. Scholberg, "Prospects for measuring coherent neutrino-nucleus elastic scattering at a stopped-pion neutrino source," *Physical Review D: Particles, Fields, Gravitation and Cosmology*, vol. 73, Article ID 033005, 2006.

[58] W. Grimus, M. Maltoni, T. Schwetz, M. A. Tortola, and J. W. F. Valle, "Constraining Majorana neutrino electromagnetic properties from the LMA-MSW solution of the solar neutrino problem," *Nuclear Physics B*, vol. 648, no. 1-2, pp. 376–396, 2003.

[59] B. Cañas, O. Miranda, A. Parada, M. Tórtola, and J. Valle, "Addendum to "Updating neutrino magnetic moment constraints," *Physics Letters B*, vol. 757, p. 568, 2016.

[60] J. B. Dent, B. Dutta, S. Liao, J. L. Newstead, L. E. Strigari, and J. W. Walker, "Probing light mediators at ultralow threshold energies with coherent elastic neutrino-nucleus scattering," *Physical Review D: Particles, Fields, Gravitation and Cosmology*, vol. 96, no. 9, 2017.

[61] I. M. Shoemaker, "A COHERENT Search Strategy for Beyond Standard Model Neutrino Interactions," *Physical Review D: Particles, Fields, Gravitation and Cosmology*, vol. 95, Article ID 115028, 2017.

[62] M. Lindner, W. Rodejohann, and X.-J. Xu, "Coherent Neutrino-Nucleus Scattering and new Neutrino Interactions," *Journal of High Energy Physics*, vol. 3, no. 97, 2017.

[63] D. G. Cerdeño, M. Fairbairn, T. Jubb, P. A. Machado, A. C. Vincent, and C. Bœhm, "Erratum to: Physics from solar neutrinos in dark matter direct detection experiments," *Journal of High Energy Physics*, vol. 2016, no. 9, 2016.

[64] J. Liao and D. Marfatia, "COHERENT constraints on nonstandard neutrino interactions," *Physics Letters B*, vol. 775, pp. 54–57, 2017.

[65] V. Antonelli, L. Miramonti, C. Pena Garay, and A. Serenelli, "Solar Neutrinos," https://arxiv.org/abs/1208.1356.

[66] G. Bellini, J. Benziger, and D. Bick, "Neutrinos from the primary proton-proton fusion process in the Sun," *Nature*, vol. 512, no. 7515, pp. 383–386, 2014.

[67] S. Horiuchi, J. F. Beacom, and E. Dwek, "Diffuse supernova neutrino background is detectable in Super-Kamiokande," *Physical Review D: Particles, Fields, Gravitation and Cosmology*, vol. 79, no. 8, 2009.

[68] D. P. Ahalpara, K. H. Bhatt, and R. Sahu, "Collective bands in 81Sr," *Journal of Physics G: Nuclear and Particle Physics*, vol. 11, no. 6, pp. 735–743, 1985.

[69] L. Coraggio, L. De Angelis, T. Fukui, A. Gargano, and N. Itaco, "Calculation of Gamow-Teller and two-neutrino double-β decay properties for 130Te and 136Xe with a realistic nucleon-nucleon potential," *Physical Review C*, vol. 59, Article ID 064324, 2018.

[70] R. Sahu and V. K. B. Kota, "Deformed shell model for T=0 and T=1 bands in 62Ga and 66As," *Physical Review C*, vol. 66, Article ID 024301, 2002.

[71] R. Sahu and V. K. B. Kota, "Deformed shell model for collective T=0 and T=1 bands in 46V and 50Mn," *Physical Review C*, vol. 67, Article ID 054323, 2003.

[72] P. C. Srivastava, R. Sahu, and V. K. B. Kota, "Shell model and deformed shell model spectroscopy of 62Ga," *The European Physical Journal A*, vol. 51, no. 3, 2015.

[73] B. Ding et al., "High-spin states in ^{127}I," *Physical Review C*, vol. 85, Article ID 044306, 2012.

[74] A. Beda, V. Brudanin, V. Egorov et al., "The results of search for the neutrino magnetic moment in GEMMA experiment," *Advances in High Energy Physics*, vol. 2012, Article ID 350150, 12 pages, 2012.

[75] J. Billard, J. Johnston, and B. J. Kavanagh, "Prospects for exploring New Physics in Coherent Elastic Neutrino-Nucleus Scattering," https://arxiv.org/abs/1805.01798.

[76] M. Abdullah, J. B. Dent, B. Dutta, G. L. Kane, S. Liao, and L. E. Strigari, "Coherent Elastic Neutrino Nucleus Scattering (CEνNS) as a probe of Z$\prime$ through kinetic and mass mixing effects," *Physical Review D*, vol. 98, Article ID 015005, 2018.

[77] M. Abdullah, M. Dalchenko, B. Dutta et al., "Bottom-quark Fusion Processes at the LHC for Probing Z$\prime$ Models and B-meson Decay Anomalies," *Physical Review D*, vol. 97, Article ID 075035, 2018.

[78] Y. Farzan, "A model for large non-standard interactions of neutrinos leading to the LMA-Dark solution," *Physics Letters B*, vol. 748, pp. 311–315, 2015.

[79] P. Coloma, P. B. Denton, M. C. Gonzalez-Garcia, M. Maltoni, and T. Schwetz, "Curtailing the dark side in non-standard neutrino interactions," *Journal of High Energy Physics*, vol. 2017, no. 4, 2017.